

Communication between the Zinc and Tetrahydrobiopterin Binding Sites in Nitric Oxide Synthase

Georges Chreifi,[†] Huiying Li,[†] Craig R. McInnes,^{||} Colin L. Gibson,^{||} Colin J. Suckling,^{||} and Thomas L. Poulos*,^{†,‡,§}

Departments of [†]Molecular Biology and Biochemistry, [‡]Chemistry, and [§]Pharmaceutical Sciences, University of California, Irvine, California 92697-3900, United States

^{||}WestCHEM, Department of Pure and Applied Chemistry, University of Strathclyde, 295 Cathedral Street, Glasgow G1 1XL, Scotland, U.K.

ABSTRACT: The nitric oxide synthase (NOS) dimer is stabilized by a Zn²⁺ ion coordinated to four symmetry-related Cys residues exactly along the dimer 2-fold axis. Each of the two essential tetrahydrobiopterin (H₄B) molecules in the dimer interacts directly with the heme, and each H₄B molecule is ~15 Å from the Zn²⁺. We have determined the crystal structures of the bovine endothelial NOS dimer oxygenase domain bound to three different pterin analogues, which reveal an intimate structural communication between the H₄B and Zn²⁺ sites. The binding of one of these compounds, 6-acetyl-2-amino-7,7-dimethyl-7,8-dihydro-4(3H)-pteridinone (**1**), to the pterin site and Zn²⁺ binding are mutually exclusive. Compound **1** both directly and indirectly disrupts hydrogen bonding between key residues in the Zn²⁺ binding motif, resulting in destabilization of the dimer and a complete disruption of the Zn²⁺ site. Addition of excess Zn²⁺ stabilizes the Zn²⁺ site at the expense of weakened binding of **1**. The unique structural features of **1** that disrupt the dimer interface are extra methyl groups that extend into the dimer interface and force a slight opening of the dimer, thus resulting in disruption of the Zn²⁺ site. These results illustrate a very delicate balance of forces and structure at the dimer interface that must be maintained to properly form the Zn²⁺, pterin, and substrate binding sites.

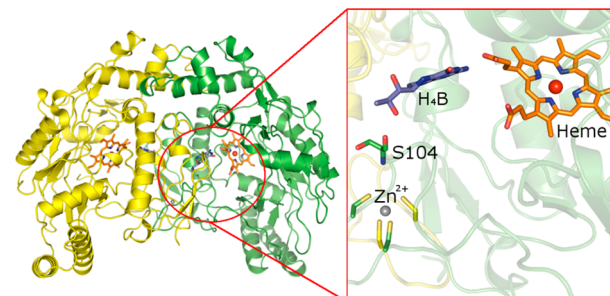
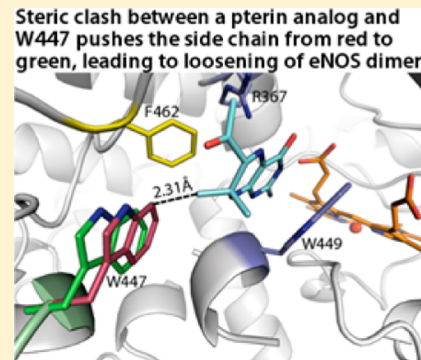


Figure 1. Overall structure of the bovine eNOS dimer in complex with H₄B (Protein Data Bank entry 9NSE). The Zn²⁺ binding site is located at the dimer interface and ~15 Å from the center of the pterin binding pocket in both molecules A and B of the dimer. Chain A is colored green, chain B yellow, pterin blue, and heme orange. All structural figures were prepared with PyMol (<http://www.pymol.org>).

nNOS to iNOS and that the role of H₄B in dimer stability is less critical in eNOS.^{15,16} The structural basis for this disparity, however, is not yet fully understood.

One way of exploring the relationship between dimer stability and H₄B binding is to investigate the pterin binding

Received: April 2, 2014

Revised: May 10, 2014

Published: May 12, 2014

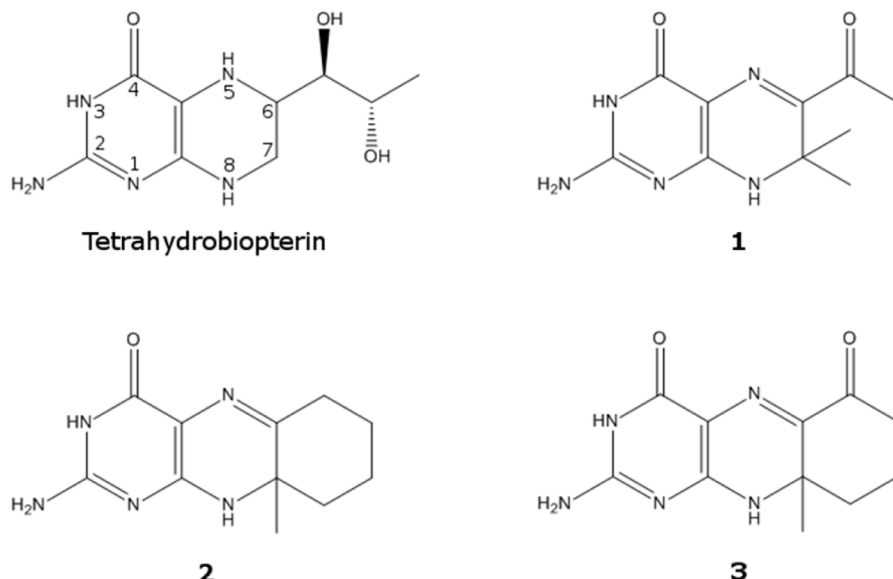


Figure 2. Chemical structures of the pterin compounds. **1–3** were designed and synthesized to be the dihydro analogues of NOS cofactor H₄B.

pocket using various pterin analogues. Moreover, inactive pterin analogues could potentially serve as NOS inhibitors^{12,17–19} and have proven to be useful in probing the function of H₄B.^{20–23} In this study, we have determined the crystal structures of three novel pterin compounds (Figure 2) analogous to H₄B bound to eNOS, which has unexpectedly provided important insights into the intimate connection among the Zn²⁺, pterin, and substrate binding sites.

MATERIALS AND METHODS

Protein Expression and Purification. The bovine holo-eNOS pCWori construct containing an *Amp^R* gene and an N-terminal six-His tag was expressed in *Escherichia coli* BL21-(DE3) cells already containing the calmodulin plasmid (with a *Chl^R* gene), and the cells were then plated on LB agar with ampicillin (100 µg/mL) and chloramphenicol (35 µg/mL). *E. coli* cells inherently lack the machinery to synthesize H₄B, ensuring that eNOS would remain free of H₄B. A single colony was used to inoculate each 5 mL of LB starter culture (100 µg/mL ampicillin and 35 µg/mL chloramphenicol). The culture was incubated for 8 h at 37 °C with 220 rpm agitation. Each liter of TB medium (100 µg/mL ampicillin and 35 µg/mL chloramphenicol) was inoculated with 2 mL of LB starter culture. The cells were grown at 37 °C with agitation at 220 rpm until the OD (600 nm) reached 1.0–1.2. Protein expression was then induced by adding 0.5 mM isopropyl β-D-thiogalactoside and 0.4 mM δ-aminolevulinic acid. New doses of ampicillin and chloramphenicol were also added, and cell growth resumed at 25 °C and 100 rpm for 24 h. The cells were then harvested by centrifugation and stored at –80 °C.

Cells were thawed and resuspended by being stirred for 3 h at 4 °C in buffer A [50 mM sodium phosphate (pH 7.8), 10% glycerol, 0.5 mM L-Arg, 5 mM β-mercaptoethanol, 0.1 mM phenylmethanesulfonyl fluoride (PMSF), and 200 mM NaCl]. The following protease inhibitors were added to buffer A before lysis: trypsin inhibitor (5 µg/mL), pepstatin A (1 µg/mL), and leupeptin (1 µg/mL). Cells were lysed by being passed through a microfluidizer at 18K psi (Microfluidics International Co.). The soluble fraction was isolated by centrifugation at 17000 rpm and 4 °C for 1 h. The crude extract was then loaded onto a

Ni²⁺-nitrilotriacetate column pre-equilibrated with 10 bed volumes of buffer A. After being loaded with the crude extract, the column was washed with 10 bed volumes of 10 mM imidazole in buffer A before being eluted with a 10 to 200 mM imidazole linear gradient in buffer A. Colored fractions were pooled and loaded onto a 2',5'-ADP Sepharose column pre-equilibrated with buffer B [50 mM Tris-HCl (pH 7.8), 10% glycerol, 5 mM β-mercaptoethanol, 0.1 mM PMSF, 0.5 mM L-Arg, and 200 mM NaCl]. The column was then washed with 10 bed volumes of buffer B and eluted with 10 mM NADP⁺ in buffer B. Colored fractions were pooled and concentrated in a 30000 molecular weight cutoff (MWCO) Amicon concentrator at 4 °C. The eNOS heme domain used for crystallization was generated by limited trypsinolysis: a 20:1 eNOS:trypsin weight ratio was used for a 1 h incubation at 25 °C. The digested sample was then loaded onto a Superdex 200 column (HiLoad 26/60, GE Healthcare) controlled by an FPLC system and pre-equilibrated with buffer B to separate the heme domain and flavin-containing fragment generated by the trypsin digest. Fractions were pooled according to an *A*₂₈₀/*A*₃₉₅ spectral ratio of <1.7, and sample homogeneity was determined by SDS-PAGE.

Synthesis of H₂B Analogues. The preparation of pterin compounds 6-acetyl-2-amino-7,8-dimethyl-7,8-dihydro-4(3H)-pteridinone (**1** in Figure 2), 2-amino-9a-methyl-6,7,8,9a,10-hexahydrobenzo[g]pteridin-4(3H)-one (**2**), and 2-amino-9a-methyl-8,9,9a,10-tetrahydrobenzo[g]pteridine-4,6(3H,7H)-dione (**3**) used in this study has been previously described.^{24,25}

Crystal Preparation. All eNOS heme domain samples were prepared for crystallization by being concentrated to 12 mg/mL in buffer B using a 30000 MWCO Amicon concentrator. Cocrystallization was conducted by combining protein with 5 mM cofactor and 5 mM L-arginine. Crystals were grown at 4 °C in 18–20% PEG 3350 (w/v), 250 mM magnesium acetate, 100 mM cacodylate (pH 6.25), and 5 mM tris(2-carboxyethyl)-phosphine (TCEP) in a sitting-drop vapor diffusion setup. Freshly grown crystals were passed stepwise through a cryoprotectant solution containing 20% PEG 3350, 10% (v/v) glycerol, 10% (w/v) trehalose, 5% (w/v) sucrose, 5% (w/v)

Table 1. Crystallographic Data and Refinement Statistics

	1	2	3	1 (with 50 μ M Zn acetate)
PDB entry	4CUL	4CUM	4CUN	4CVG
radiation source	SSRL BL 7-1	SSRL BL 7-1	SSRL BL 7-1	SSRL BL 9-2
space group	$P_{2_1}2_12_1$	$P_{2_1}2_12_1$	$P_{2_1}2_12_1$	$P_{2_1}2_12_1$
unit cell dimensions a, b, c (\AA)	57.09, 105.47, 158.25	58.01, 106.49, 156.48	58.87, 106.18, 156.74	57.41, 105.96, 156.53
data resolution (\AA) (highest-resolution shell)	50.0–2.23 (2.31–2.23)	88.04–2.33 (2.41–2.33)	87.9–2.48 (2.57–2.48)	50.0–2.31 (2.39–2.31)
X-ray wavelength (\AA)	1.13	1.13	1.13	0.98
total no. of observations	208127	184003	140206	164961
no. of unique reflections (highest-resolution shell)	47234 (4613)	42159 (4091)	35505 (3482)	42009 (3784)
completeness (%) (highest-resolution shell)	99.77 (98.99)	99.53 (97.87)	99.47 (99.63)	97.91 (90.01)
R_{merge} (highest-resolution shell)	0.088 (0.884)	0.085 (0.862)	0.078 (0.689)	0.060 (0.690)
I/σ (highest-resolution shell)	19.86 (2.01)	22.03 (2.13)	22.85 (2.01)	24.04 (2.07)
redundancy (highest-resolution shell)	4.4 (4.4)	4.4 (4.4)	3.9 (3.8)	4.0 (3.9)
B factor, Wilson plot (\AA^2)	38.83	44.96	56.81	43.54
no. of protein atoms	6141	6446	6446	6400
no. of heteroatoms	158	169	173	131
no. of waters	279	214	51	231
disordered residues	40–66, 91–120 (A) 40–68, 91–120 (B)	40–66, 110–120 (A) 40–68, 112–120 (B)	40–66, 110–120 (A) 40–68, 112–120 (B)	40–66, 108–120 (A) 40–68, 109–120 (B)
$R_{\text{work}}/R_{\text{free}}$	0.165/0.209	0.170/0.227	0.184/0.242	0.155/0.214
root-mean-square deviation for bond lengths (\AA)	0.012	0.017	0.017	0.017
root-mean-square deviation for bond angles (deg)	1.47	1.69	1.97	1.83

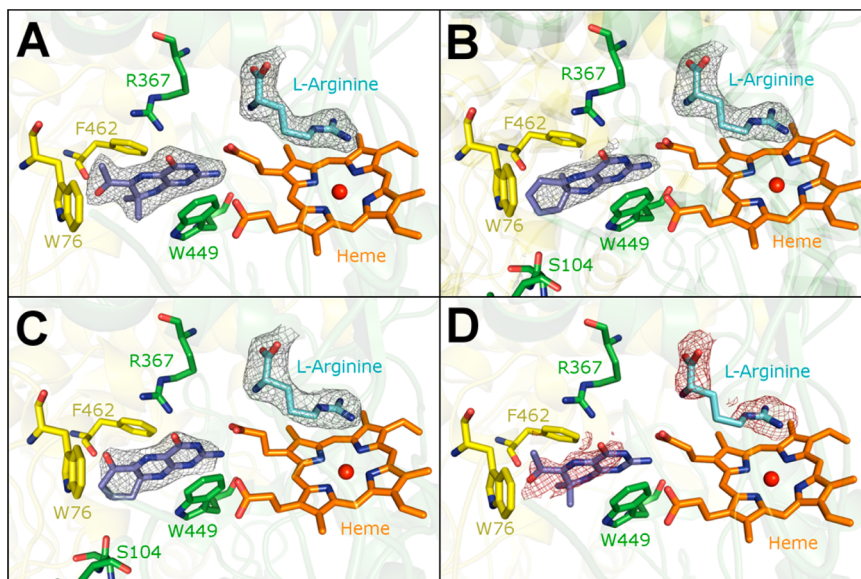


Figure 3. (A) Active site of bovine eNOS in complex with pterin analogue 1 with the $2F_o - F_c$ electron density map contoured at 1.0σ . The strong density supports binding to the pterin site even though the compound lacks the ability to form a hydrogen bond with Ser104 of chain A. (B and C) Active site of bovine eNOS in complex with 2 and 3, respectively, with the $2F_o - F_c$ density map contoured at 1.0σ . The density for 2 is not as strong as that for analogue 1 but supports binding of 2 with the extra methyl facing F462, while the density for 3 is weaker than that for 1 or 2 yet strong enough to support binding of 3 in the shown orientation. (D) Active site of bovine eNOS in complex with pterin analogue 1 as shown in panel A but overlaid with the $2F_o - F_c$ map (1.0σ) calculated using the data collected with a crystal supplemented with 50 μM Zn acetate during the cryoprotectant soaks. The poorly defined pterin and substrate density at best supports partial occupancy. The color scheme for this figure and Figure 4 is as follows: Chain A is colored green, chain B yellow, pterin blue, substrate L-arginine cyan, and the heme orange.

mannitol, 10 mM cofactor, and 5–10 mM L-Arg for 4–6 h at 4 °C before being flash-cooled with liquid nitrogen.

X-ray Diffraction Data Collection, Processing, and Structure Refinement. Cryogenic (100 K) X-ray diffraction data were collected remotely at Stanford Synchrotron Radiation Lightsource (SSRL) using the data collection control software Blu-Ice²⁶ and a crystal mounting robot. An ADSC Q315r CCD

detector at beamline 7-1 or a Mar325 CCD detector at beamline 9-2 was used for data collection. Raw data frames were indexed, integrated, and scaled using HKL2000.²⁷ The binding of H₄B cofactors was detected by the initial difference Fourier maps calculated with REFMAC.²⁸ The pterin molecules were then modeled in COOT²⁹ and refined using REFMAC. Water molecules were added in REFMAC and

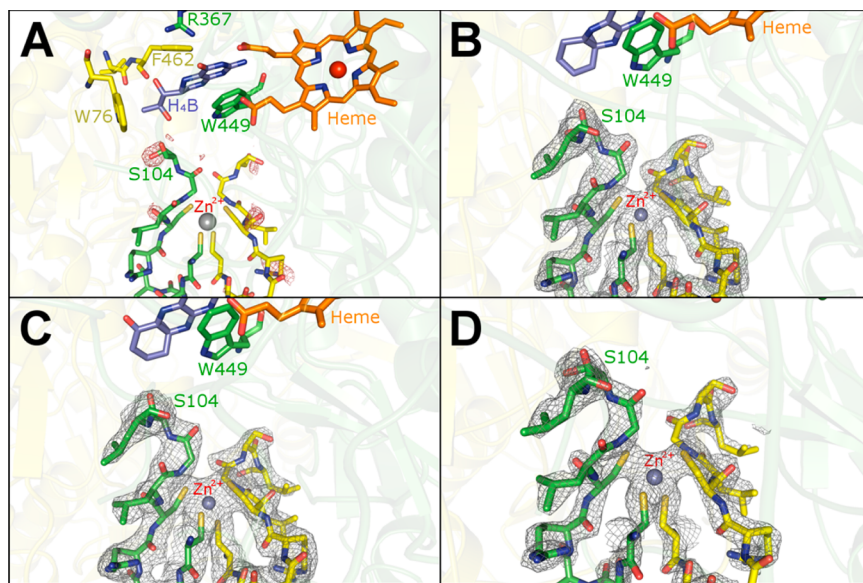


Figure 4. (A) $2F_o - F_c$ electron density map (at the 1.0σ contour level) from the eNOS-1 complex structure overlaid on a reference bovine eNOS structure with bound H_4B and an ordered Zn^{2+} site (PDB entry 9NSE). This is to illustrate the disordered Zn^{2+} site resulting from binding of compound **1** to the pterin pocket. The lack of electron density spans residues 91–109 in chain A and residues 91–111 in chain B. (B and C) Zn^{2+} binding site of bovine eNOS in complex with **2** and **3**, respectively. The $2F_o - F_c$ density map is at a contour level of 1.0σ and shows a fully ordered Zn^{2+} site, supporting undisrupted Zn^{2+} binding. (D) $2F_o - F_c$ density map for the Zn^{2+} binding site at a contour level of 1.0σ derived from the same eNOS-1 structure showing poor pterin and substrate density in Figure 3D. The crystal was soaked in a cryoprotectant solution supplemented with $50\ \mu M$ Zn acetate. The Zn^{2+} site is fully ordered, while compound **1** is disordered in structure.

checked by COOT. The TLS³⁰ protocol was implemented in the final stage of refinements with each subunit as one TLS group. The refined structures were validated in COOT before being deposited in the Protein Data Bank. The crystallographic data collection and structure refinement statistics are listed in Table 1 with Protein Data Bank (PDB) entry codes included.

RESULTS AND DISCUSSION

Structural Characterization of the H_4B Binding Pocket

Pocket. As shown in Figure 2, the three dihydropterin analogues retain the ring structure of H_4B and introduce variations only in the side chain. Figure 3 shows the electron density of the three dihydropterin analogues bound to eNOS. Compound **1** (Figure 3A) exhibits the strongest and most well-defined electron density. As expected from its structural similarity to H_4B , compound **1** fits into the pterin binding pocket quite well, maintaining most of the interactions found with H_4B : the π - π stacking with W449, the H-bonds from its 2-aminopyrimidine nitrogens to the heme propionate A, the H-bond from O4 to R367, and the van der Waals contacts with aromatic residues of the other subunits (W76 and F462). Therefore, it is not surprising that the tetrahydro form of **1** can support the conversion of L-arginine to NO in nNOS.³¹ From kinetic studies, the estimated K_D for **1** is $115\ \mu M$ compared to a value of $1.1\ \mu M$ for H_4B .³¹

However, the two additional H-bonds from the dihydroxypropyl side chain of H_4B to the carbonyls of S104 and F462 are lost in **1**. Unique to **1** is the close contact from one of its methyl groups at the C7 position to the W447 side chain of the other subunit. Both **2** and **3** in the dihydro oxidation state introduce a third cyclohexane ring to replace the H_4B side chain. Although the third ring is tolerated by the pterin binding pocket, the extra methyl group at C7 may generate steric clashes with the protein. As a result, **2** (Figure 3B) and **3** (Figure 3C) exhibit weaker electron density. Crystals of the

eNOS-3 complex diffract poorly, which we have found correlates well with poor ligand binding. Because **3** is structurally similar to **2** and differs only in the carbonyl O atom on the cyclohexane ring, the additional steric crowding of this oxygen in **3** very likely accounts for why this pterin analogue binds more poorly. Overall, the inability of the three pterin analogues to form hydrogen bonds with S104 and F462 and the steric clashes from their protruding methyl groups may be attributed to a binding affinity that is poorer than that of the native pterin, H_4B .

Disruption of the Zn^{2+} Binding Site. As shown in Figure 4, a single Zn^{2+} ion is situated at the dimer interface where it is tetrahedrally coordinated by symmetry-related Cys residues along the dimer axis. The Zn^{2+} is $\sim 15\ \text{\AA}$ from the center of the pterin binding pocket in both subunits A and B of the dimer. Quite unexpectedly, we found that the binding of **1** completely disrupts the Zn^{2+} binding region, as evidenced by a total lack of electron density for residues 91–109 and the Zn^{2+} (Figure 4A). It has been known for some time that both Zn^{2+} and H_4B contribute to dimer stability,^{8,32,33} but this is the first indication that there is a relatively long-range communication between these two sites. To probe whether the binding of **1** and the binding of Zn^{2+} are mutually exclusive, we soaked crystals of the eNOS-1 complex in a cryoprotectant solution supplemented with $50\ \mu M$ Zn acetate. The crystal structure shows that Zn^{2+} binding is restored (Figure 4D), while the electron density for **1** and the substrate, L-Arg, are poorly defined (Figure 3D). We next soaked crystals at a more moderate Zn acetate concentration of $20\ \mu M$. In this case, **1** and L-Arg bind well but the Zn^{2+} site is disordered (data not shown). In contrast, binding of **2** and binding of **3** do not interfere with Zn^{2+} binding (Figure 4B,C). The interdependence of pterin and L-Arg binding is well-known and is very likely mediated by the fact H_4B H-bonds to the same heme propionate as the α -amino group of L-Arg (Figure 3).^{12–14}

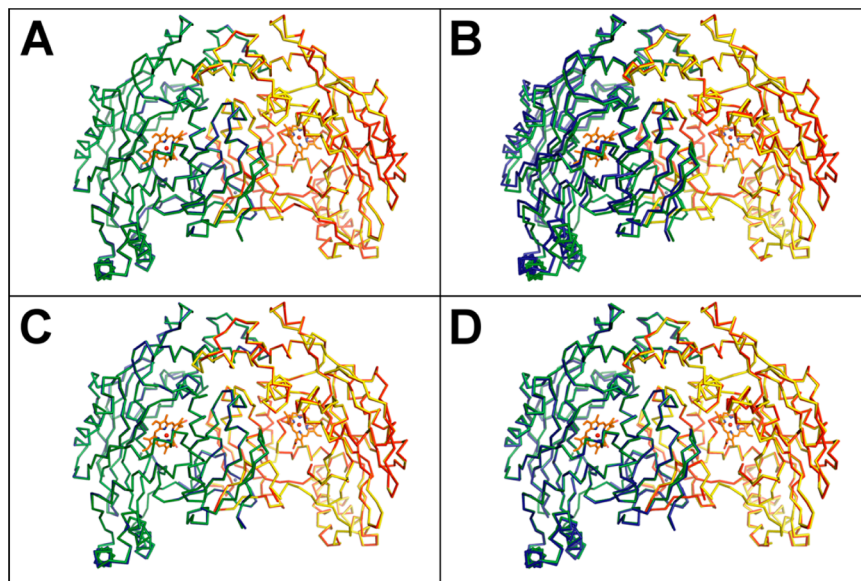


Figure 5. (A) Superposition of the α -carbon backbone of an H_4B -free (PDB entry 5NSE) on an H_4B -bound (PDB entry 9NSE) eNOS heme domain structure. For all four panels, the superposition was conducted in Coot only on chain A of both structures to observe the relative deviation in chain B. The color scheme is as follows. For the H_4B -bound structure, chain A is colored yellow and chain B green. For the H_4B -free or pterin analogue-bound structures, chain A is colored red and chain B blue. (B–D) Superposition of an H_4B -bound eNOS heme domain (PDB entry 9NSE) with a compound 1, 2, and 3 bound structure, respectively.

How Does the Pterin Site Communicate with the Zn^{2+} Site? These results clearly show that there is a strong long-range communication between the Zn^{2+} , pterin, and substrate binding sites. To explain why, we next conducted a detailed comparison between the eNOS–1 complex with a disordered Zn^{2+} and the fully ordered eNOS structure with H_4B bound. By superposition of the α -carbon backbone of chains A (Figure 5B), we see that chain B has shifted away by a significant distance. For comparison, we next superposed H_4B -bound to H_4B -free eNOS structures (Figure 5A) and did the same for bound structures of 2 (Figure 5C) and 3 (Figure 5D). In these cases, chain B does not move significantly relative to chain A. For the sake of consistency, we superposed the α -carbon backbone of chain B and observed a similar shift in chain A. To further quantify the observation, we calculated the root-mean-square deviations (rmsds) of chains A and B for residues 121–482 in each pair of structures. For the eNOS–1 complex superposed on the basis of only chain A with an H_4B -bound eNOS reference structure (PDB entry 9NSE), the rmsd of chain B is 1.23 Å, compared to the values of 0.27–0.44 Å calculated with the same method against the same reference structure for either an H_4B -free structure or other pterin analogue structures that do not disrupt the Zn^{2+} site (Table 2).

A close examination of the eNOS–1 structure reveals that chain B moves away from chain A because of the methyl groups on C7 of 1 (Figure 6B). Accommodating these methyl substituents forces W447 of chain B to shift away from chain A. The shift of W447 is not merely absorbed locally, but instead induces a global change in the entire chain B as a rigid body. The repulsion between the methyl group of 1 and W447 occurs in a symmetrical manner in both subunits, resulting in the slight opening of the dimer interface. The widened dimer interface causes disruption of key backbone contacts between the Cys-bearing Zn^{2+} binding hairpin fragment (residues 95–102) that includes contacts between C101 and N468 (Figure 6B). Loss of those key interactions leads to the total disordering of the Zn^{2+} binding site. Comparatively, the H_4B -free eNOS structure

Table 2. Calculation of Root-Mean-Square Deviations of α -Carbons^a

structure	PDB entry	root-mean-square deviation (Å)	
		chain A	chain B
H_4B -free	5NSE	0.165	0.357
compound 1	4CUL	0.250	1.227
compound 2	4CUM	0.220	0.270
compound 3	4CUN	0.309	0.418
compound 1 (with 50 μM Zn acetate)	4CVG	0.218	0.446

^aChain A of each structure was superposed with chain A of H_4B -bound eNOS (PDB entry 9NSE), and all rmsds were calculated using LSQMAN (<http://xray.bmc.uu.se/usf/>).

(Figure 6A) and those in complexes with 2 (Figure 6C) and 3 (Figure 6D) show practically no shift of W447. The extra methyl group in 2 and 3 is not directly pointing to W447, causing no disruption of the dimer interface. In the same way, we also compared the H_4B -bound eNOS structure to the structure of the eNOS–1 complex supplemented with 50 μM Zn^{2+} giving a restored Zn^{2+} site, and the resulting superposition shows a tighter dimer (Figure 7A) and a restored W447 position (Figure 7B) at the expense of weakened binding of 1 (Figure 3D). It also should be noted that residues directly contacting H_4B , W447, W449, and F462, are conserved in both nNOS and eNOS.

What Does This Communication Reveal about the NOS Dimer? These results reveal that the eNOS dimer is able to loosen up and expand to accommodate 1. The side effect is that all hydrogen bonding interactions that stabilize the Zn^{2+} binding site, mainly the two between N468 and C101, are weakened or lost, as shown in Figure 6. This effect being compounded on both chains causes a complete disruption of Zn^{2+} binding and destabilization of the dimer.

Previous studies have shown that eNOS has the most stable dimer compared to nNOS and iNOS.¹⁶ To obtain NOS–pterin

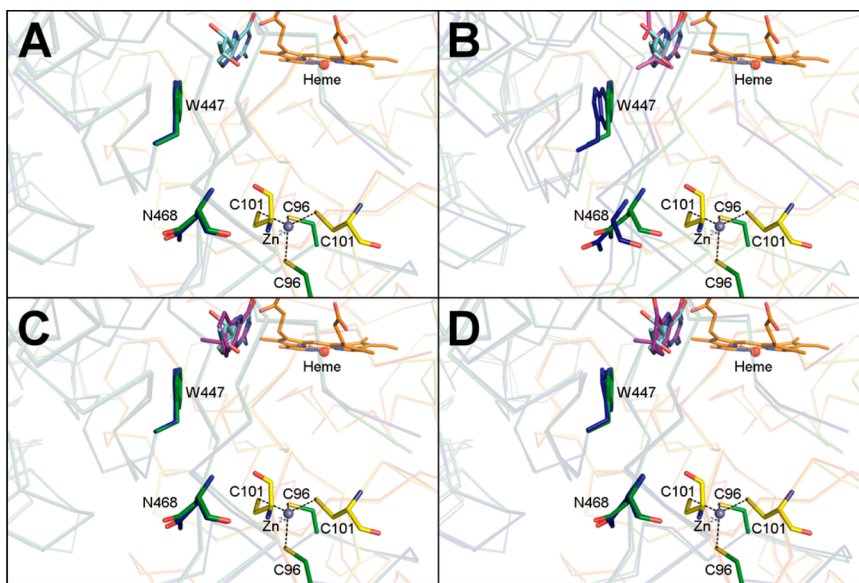


Figure 6. Close-up views based on the same superpositions shown in Figure 5 for observation of the relative structural deviation of W447 of chain B for each pair of structures: (A) eNOS with or without H_4B bound, (B) H_4B vs compound 1, (C) H_4B vs compound 2, and (D) H_4B vs compound 3. The color scheme for all four panels is as follows. For the H_4B -bound form, chain A is colored yellow and chain B green. For the H_4B -free or pterin analogue-bound structures, chain A is colored red and chain B blue. H_4B is colored cyan, the pterin analogue purple, and the heme orange.

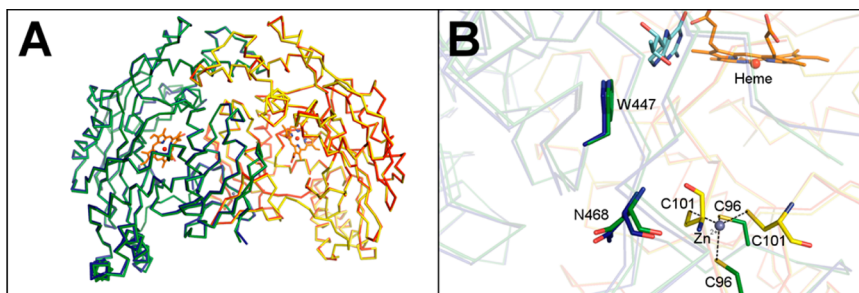


Figure 7. (A) Superposition of the α -carbon backbone of eNOS heme domains with compound 1 bound, supplemented with $50 \mu\text{M}$ Zn acetate in a cryosoak, on an H_4B -bound structure (PDB entry 9NSE). The superposition was done only on chain A of both structures to observe the relative deviation in chain B. (B) Close-up view of the Zn^{2+} binding and active sites based on the superposition in panel A for the observation of the relative structural deviation of W447 in chain B. The color scheme for both panels is as follows. For the H_4B -bound form, chain A is colored yellow and chain B green. For the pterin analogue-bound form, chain A is colored red and chain B blue. H_4B is colored cyan, the pterin analogue purple, and the heme orange.

complexes, it is necessary to purify NOS in the absence of H_4B and only eNOS, not nNOS, is stable enough without H_4B during purification and the proteolysis required to generate the heme domain for crystallization. Two attempts were made to purify nNOS with pterin-free buffer or the buffer supplemented with 1, but the protein denatured completely upon trypsinolysis required for generating the heme domain. This very likely reflects the fact that the eNOS dimer is more stable than nNOS: it can survive purification without H_4B bound and can bind 1 without disruption of the dimer. This also suggests that the combination of intersubunit contacts attributed to the greater dimer strength of eNOS allows it to survive disruption of the Zn^{2+} site without complete disruption of the dimer.

SUMMARY

Even though the importance of H_4B in stabilizing the NOS dimer has been known for some time, this study provides the structural basis for the intimate structural communication among H_4B , Zn^{2+} , substrate binding, and dimer stability. It is important to note that zinc-free NOS retains near full catalytic

activity, although the dimer is substantially less stable.³³ A number of biochemical studies^{32,34–37} have shown that the main role of the zinc site is to promote H_4B binding, which in turn increases the affinity for the substrate, L-Arg. The study presented here provides a structural basis for this interdependence. We were fortunate that the additional stability of the eNOS dimer allowed us to probe perturbations at the dimer interface without totally disrupting the dimer, which would preclude any detailed crystallographic analysis as in the case of nNOS. It is remarkable that the mere addition of the methyl groups in 1 can have such a dramatic effect on the Zn^{2+} site. This underscores the exquisite fine-tuning of interactions that stabilize the NOS dimer and the close interdependence of the Zn^{2+} , pterin, and substrate binding sites.

ASSOCIATED CONTENT

Accession Codes

Coordinates and structure factors have been deposited in the Protein Data Base as entries 4CUL, 4CUM, 4CUN, and 4CVG.

AUTHOR INFORMATION

Corresponding Author

*E-mail: poulos@uci.edu. Phone: (949) 824-7020.

Funding

This work was supported by National Institutes of Health Grant GM57353 (T.L.P.).

Notes

The authors declare no competing financial interest.

ACKNOWLEDGMENTS

We thank Dr. Sarvind M. Tripathi for helpful discussions and suggestions as well as the beamline staff at the Stanford Synchrotron Radiation Lightsource for their assistance during X-ray diffraction data collection.

REFERENCES

- (1) Hevel, J. M., White, K. A., and Marletta, M. A. (1991) Purification of the inducible murine macrophage nitric oxide synthase. Identification as a flavoprotein. *J. Biol. Chem.* 266, 22789–22791.
- (2) Marletta, M. A. (1993) Nitric oxide synthase structure and mechanism. *J. Biol. Chem.* 268, 12231–12234.
- (3) Stuehr, D. J., and Griffith, O. W. (1992) Mammalian nitric oxide synthases. *Adv. Enzymol. Relat. Areas Mol. Biol.* 65, 287–346.
- (4) Forstermann, U., and Sessa, W. C. (2012) Nitric oxide synthases: Regulation and function. *Eur. Heart J.* 33, 829–837 , 837a–837d.
- (5) Knowles, R. G., and Moncada, S. (1994) Nitric oxide synthases in mammals. *Biochem. J.* 298, 249–258.
- (6) Crane, B. R., Arvai, A. S., Gachhui, R., Wu, C., Ghosh, D. K., Getzoff, E. D., Stuehr, D. J., and Tainer, J. A. (1997) The structure of nitric oxide synthase oxygenase domain and inhibitor complexes. *Science* 278, 425–431.
- (7) Raman, C. S., Li, H., Martasek, P., Kral, V., Masters, B. S., and Poulos, T. L. (1998) Crystal structure of constitutive endothelial nitric oxide synthase: A paradigm for pterin function involving a novel metal center. *Cell* 95, 939–950.
- (8) Li, H., Raman, C. S., Glaser, C. B., Blasko, E., Young, T. A., Parkinson, J. F., Whitlow, M., and Poulos, T. L. (1999) Crystal structures of zinc-free and -bound heme domain of human inducible nitric-oxide synthase. Implications for dimer stability and comparison with endothelial nitric-oxide synthase. *J. Biol. Chem.* 274, 21276–21284.
- (9) Wei, C. C., Wang, Z. Q., Wang, Q., Meade, A. L., Hemann, C., Hille, R., and Stuehr, D. J. (2001) Rapid kinetic studies link tetrahydrobiopterin radical formation to heme-dioxy reduction and arginine hydroxylation in inducible nitric-oxide synthase. *J. Biol. Chem.* 276, 315–319.
- (10) Bec, N., Gorren, A. F. C., Mayer, B., Schmidt, P. P., Andersson, K. K., and Lange, R. (2000) The role of tetrahydrobiopterin in the activation of oxygen by nitric-oxide synthase. *J. Inorg. Biochem.* 81, 207–211.
- (11) Santolini, J., Meade, A. L., and Stuehr, D. J. (2001) Differences in three kinetic parameters underpin the unique catalytic profiles of nitric-oxide synthases I, II, and III. *J. Biol. Chem.* 276, 48887–48898.
- (12) Presta, A., Siddhanta, U., Wu, C., Sennequier, N., Huang, L., Abu-Soud, H. M., Erzurum, S., and Stuehr, D. J. (1998) Comparative functioning of dihydro- and tetrahydropterins in supporting electron transfer, catalysis, and subunit dimerization in inducible nitric oxide synthase. *Biochemistry* 37, 298–310.
- (13) Klatt, P., Schmid, M., Leopold, E., Schmidt, K., Werner, E. R., and Mayer, B. (1994) The pteridine binding site of brain nitric oxide synthase. Tetrahydrobiopterin binding kinetics, specificity, and allosteric interaction with the substrate domain. *J. Biol. Chem.* 269, 13861–13866.
- (14) List, B. M., Klosch, B., Volker, C., Gorren, A. C., Sessa, W. C., Werner, E. R., Kukovetz, W. R., Schmidt, K., and Mayer, B. (1997) Characterization of bovine endothelial nitric oxide synthase as a homodimer with down-regulated uncoupled NADPH oxidase activity: Tetrahydrobiopterin binding kinetics and role of haem in dimerization. *Biochem. J.* 323, 159–165.
- (15) Venema, R. C., Ju, H., Zou, R., Ryan, J. W., and Venema, V. J. (1997) Subunit interactions of endothelial nitric-oxide synthase. Comparisons to the neuronal and inducible nitric-oxide synthase isoforms. *J. Biol. Chem.* 272, 1276–1282.
- (16) Panda, K., Rosenfeld, R. J., Ghosh, S., Meade, A. L., Getzoff, E. D., and Stuehr, D. J. (2002) Distinct dimer interaction and regulation in nitric-oxide synthase types I, II, and III. *J. Biol. Chem.* 277, 31020–31030.
- (17) Werner, E. R., Pitters, E., Schmidt, K., Wachter, H., Werner-Felmayer, G., and Mayer, B. (1996) Identification of the 4-amino analogue of tetrahydrobiopterin as a dihydropteridine reductase inhibitor and a potent pteridine antagonist of rat neuronal nitric oxide synthase. *Biochem. J.* 320, 193–196.
- (18) Mayer, B., Wu, C., Gorren, A. C., Pfeiffer, S., Schmidt, K., Clark, P., Stuehr, D. J., and Werner, E. R. (1997) Tetrahydrobiopterin binding to macrophage inducible nitric oxide synthase: Heme spin shift and dimer stabilization by the potent pterin antagonist 4-amino-tetrahydrobiopterin. *Biochemistry* 36, 8422–8427.
- (19) Pfeiffer, S., Gorren, A. C., Pitters, E., Schmidt, K., Werner, E. R., and Mayer, B. (1997) Allosteric modulation of rat brain nitric oxide synthase by the pterin-site enzyme inhibitor 4-aminotetrahydrobiopterin. *Biochem. J.* 328, 349–352.
- (20) Schmidt, P. P., Lange, R., Gorren, A. C., Werner, E. R., Mayer, B., and Andersson, K. K. (2001) Formation of a protonated trihydrobiopterin radical cation in the first reaction cycle of neuronal and endothelial nitric oxide synthase detected by electron paramagnetic resonance spectroscopy. *JBIC, J. Biol. Inorg. Chem.* 6, 151–158.
- (21) Gorren, A. C., Schrammel, A., Riethmuller, C., Schmidt, K., Koesling, D., Werner, E. R., and Mayer, B. (2000) Nitric oxide-induced autoinhibition of neuronal nitric oxide synthase in the presence of the autoxidation-resistant pteridine 5-methyltetrahydrobiopterin. *Biochem. J.* 347, 475–484.
- (22) Riethmuller, C., Gorren, A. C., Pitters, E., Hemmens, B., Habisch, H. J., Heales, S. J., Schmidt, K., Werner, E. R., and Mayer, B. (1999) Activation of neuronal nitric-oxide synthase by the 5-methyl analog of tetrahydrobiopterin. Functional evidence against reductive oxygen activation by the pterin cofactor. *J. Biol. Chem.* 274, 16047–16051.
- (23) Hevel, J. M., and Marletta, M. A. (1992) Macrophage nitric oxide synthase: Relationship between enzyme-bound tetrahydrobiopterin and synthase activity. *Biochemistry* 31, 7160–7165.
- (24) Alhassan, S. S., Cameron, R. J., Curran, A. W. C., Lyall, W. J. S., Nicholson, S. H., Robinson, D. R., Stuart, A., Suckling, C. J., Stirling, I., and Wood, H. C. S. (1985) Specific Inhibitors in Vitamin Biosynthesis. 7. Syntheses of Blocked 7,8-Dihydropteridines Via α -Amino Ketones. *J. Chem. Soc., Perkin Trans. 1*, 1645–1659.
- (25) Cameron, R., Nicholson, S. H., Robinson, D. H., Suckling, C. J., and Wood, H. C. S. (1985) Specific Inhibitors in Vitamin Biosynthesis. 8. Syntheses of Some Functionalized 7,7-Dialkyl-7,8-Dihydropterins. *J. Chem. Soc., Perkin Trans. 1*, 2133–2143.
- (26) McPhillips, T. M., McPhillips, S. E., Chiu, H. J., Cohen, A. E., Deacon, A. M., Ellis, P. J., Garman, E., Gonzalez, A., Sauter, N. K., Phizackerley, R. P., Soltis, S. M., and Kuhn, P. (2002) Blu-Ice and the Distributed Control System: Software for data acquisition and instrument control at macromolecular crystallography beamlines. *J. Synchrotron Radiat.* 9, 401–406.
- (27) Otwinowski, Z., and Minor, W. (1997) Processing of X-ray diffraction data collected in oscillation mode. *Methods Enzymol.* 276, 307–326.
- (28) Murshudov, G. N., Vagin, A. A., and Dodson, E. J. (1997) Refinement of Macromolecular Structures by the Maximum-Likelihood Method. *Acta Crystallogr. D53*, 240–255.
- (29) Emsley, P., and Cowtan, K. (2004) Coot: Model-building tools for molecular graphics. *Acta Crystallogr. D60*, 2126–2132.

- (30) Winn, M. D., Isupov, M. N., and Murshudov, G. N. (2001) Use of TLS parameters to model anisotropic displacements in macromolecular refinement. *Acta Crystallogr. D57*, 122–133.
- (31) Suckling, C. J., Gibson, C. L., Huggan, J. K., Morthala, R. R., Clarke, B., Kununthur, S., Wadsworth, R. M., Daff, S., and Papale, D. (2008) 6-Acetyl-7,7-dimethyl-5,6,7,8-tetrahydropterin is an activator of nitric oxide synthases. *Bioorg. Med. Chem. Lett.* 18, 1563–1566.
- (32) Miller, R. T., Martasek, P., Raman, C. S., and Masters, B. S. (1999) Zinc content of *Escherichia coli*-expressed constitutive isoforms of nitric-oxide synthase. Enzymatic activity and effect of pterin. *J. Biol. Chem.* 274, 14537–14540.
- (33) Hemmens, B., Goessler, W., Schmidt, K., and Mayer, B. (2000) Role of bound zinc in dimer stabilization but not enzyme activity of neuronal nitric-oxide synthase. *J. Biol. Chem.* 275, 35786–35791.
- (34) Chen, P. F., Tsai, A. L., and Wu, K. K. (1995) Cysteine 99 of endothelial nitric oxide synthase (NOS-III) is critical for tetrahydrobiopterin-dependent NOS-III stability and activity. *Biochem. Biophys. Res. Commun.* 215, 1119–1129.
- (35) Ghosh, D. K., Wu, C., Pitters, E., Moloney, M., Werner, E. R., Mayer, B., and Stuehr, D. J. (1997) Characterization of the inducible nitric oxide synthase oxygenase domain identifies a 49 amino acid segment required for subunit dimerization and tetrahydrobiopterin interaction. *Biochemistry* 36, 10609–10619.
- (36) Martasek, P., Miller, R. T., Liu, Q., Roman, L. J., Salerno, J. C., Migita, C. T., Raman, C. S., Gross, S. S., Ikeda-Saito, M., and Masters, B. S. (1998) The C331A mutant of neuronal nitric-oxide synthase is defective in arginine binding. *J. Biol. Chem.* 273, 34799–34805.
- (37) Rodriguez-Crespo, I., Moenne-Loccoz, P., Loehr, T. M., and Ortiz de Montellano, P. R. (1997) Endothelial nitric oxide synthase: Modulations of the distal heme site produced by progressive N-terminal deletions. *Biochemistry* 36, 8530–8538.